frontiers | Frontiers in Earth Science

TYPE Original Research
PUBLISHED 20 January 2023
DOI 10.3389/feart.2022.1017597

OPEN ACCESS

EDITED BY
Zhongping Lai,
Shantou University, China

REVIEWED BY
Yougui Song,
Institute of Earth Environment, CAS, China
Janos Kovacs,
University of Pécs, Hungary
Chong Xu,
Ministry of Emergency Management (China), China
Weiming Liu,
Institute of Mountain Hazards and Environment, CAS, China

*CORRESPONDENCE
Ping Wang,
wangping@ies.ac.cn

SPECIALTY SECTION
This article was submitted to Geohazards and Georisks, a section of the journal Frontiers in Earth Science

RECEIVED 12 August 2022
ACCEPTED 21 November 2022
PUBLISHED 20 January 2023

CITATION
Shi L, Wang P, Hu G, Ge Y, Qin J, Yang H, Wang H, Xu B and Xiao R (2023), Sedimentation and geomorphology of the Ruoergai Basin outlet reach at the source of the Yellow River: Response to the late quaternary glacial debris flow damming events.
Front. Earth Sci. 10:1017597.
doi: 10.3389/feart.2022.1017597

Sedimentation and geomorphology of the Ruoergai Basin outlet reach at the source of the Yellow River: Response to the late quaternary glacial debris flow damming events

Lingfan Shi[1], Ping Wang[1]*, Gang Hu[1], Yukui Ge[1], Jintang Qin[1], Huili Yang[1], Huiying Wang[1], Bo Xu[1] and Ruiqing Xiao[2]

[1]State Key Laboratory of Earthquake Dynamics, Institute of Geology, China Earthquake Administration, Beijing, China, [2]Sichuan Institute of Geological Engineering Investigation Group Co. Ltd., Chengdu, China

Fluvial terraces in the source of the Yellow River suggest that Ruoergai Basin was connected with the lower reach after ~10 ka, much younger than the uplift chronology of the Tibetan Plateau. In this study, the geomorphology and sedimentation of the Cairima–Ningmute River at the exit of the Ruoergai Basin were investigated. Combined with the optically stimulated luminescence dating of the sediments, the reconstructed fluvial geomorphology processes are as follows: During ~50–20 ka, coarse debris such as moraines and glacial mudflows from the Anyemaqen Shan and Xiqing Shan were unloaded to the Maqu valley in the bottleneck reach of the Ruoergai Basin outflow, causing river blockage and lake formation in the upper Ruoergai Basin; during ~20–12 ka, the headward erosion of the river accelerated from the downstream to the upstream and the barrier dam eroded, forming terraces; since ~12 ka, the Yellow River has cut through the Ruoergai Basin and has developed two levels of terraces based on lacustrine sediments. Our results suggest that glacial debris flow from the Anyemaqen Shan extensively accumulated at the basin-canyon bottleneck during the last glacial period, and when the amount of sediment accumulation exceeded the amount of river erosion, damming events occurred. The glacial-interglacial cycles during the Quaternary might generate repeated damming and cut-through of the Ruoergai Basin. The Ruoergai Basin should be connected with the lower reach before ~50 ka.

KEYWORDS

the source of the Yellow River, river terrace, Ruoergai paleolakes, the damming events, late quaternary

1 Introduction

The source of the Yellow River is in the northeastern Tibetan Plateau above the Longyang Gorge, where the first large bend of the Yellow River is present, which makes an S-shaped turn as it flows through the Ruoergai Basin (Figure 1). The extinction of paleolakes in the Ruoergai Basin and the formation of the modern drainage system of the Yellow River source are emblematic geomorphic environmental events in the northeastern Tibetan Plateau (Pan et al., 1993; Wang et al., 1995; Zhang et al., 2016; Huang et al., 2022). These events play an important role in the evolution of the paleolakes in the Ruoergai Basin, through which the Yellow River has flowed since the Late Cenozoic uplift and expansion of the Tibetan Plateau (Harkins et al., 2007; Pan et al., 2009; Craddock et al., 2010). The age of the river terraces in the downstream suggests that the Yellow River started eroding toward its source area around 500 ka ago (Craddock et al., 2010). The age of the river terraces in the Ruoergai Basin suggests that the Yellow River cut through the basin around 10–30 ka ago, and the modern Yellow River was finally established 10 ka ago (Pan et al., 1993). However, few studies have been conducted on the Yellow River in comparison to considerable number of tectonic, magnetic stratigraphy, and microgeomorphic studies that have been conducted on the northeastern margin of the Tibetan Plateau (Pan et al., 2009; Stroeven et al., 2009; Li et al., 2011; Zhang et al., 2017). Thus, most important aspects are still vague and controversial, such as the space–time evolution characteristics of the development and extinction of the Ruoergai paleolakes, the function of the two different erosion processes (i.e., river headward erosion and lakes overflow erosion) in the context of the Yellow River, the uplift of Anyemaqen Shan, and the activities of piedmont faults (Pan et al., 1993, 2009; Zheng and Wang, 1996; Zhang et al., 2018; Liu et al., 2021). Additionally the effects of glacier development in the source area on the geomorphology and the geographical environment of the basin outlet reach are unclear. Therefore, extensive research is required to verify or change the conceptual model of the evolution and mechanism of the Yellow River source water system.

In the river headward erosion model, the last change of the sedimentary facies at the surface of the earth is regarded as evidence of the Yellow River's transfixion. The time taken for transition from lake to swamp is about 10 ka and that from lake to river varies greatly, ranging from 20 to 125 ka (Zhou, 1959; Zong et al., 1985; Wang et al., 1995; Wu et al., 1997; Sheng et al., 2007). However, the deep and shallow drilling data from the Ruoergai Basin provide more information on the temporal and spatial changes of the sedimentary facies. The RH and RM cores from the downstream of the Heihe River in the northern part of the basin show that sedimentation has occurred since ~1 Ma (Chen et al., 1995; Wang et al., 1995). The sedimentary lithology of the RM core is fine, with no coarse clastic sediments above medium sand (Xue et al., 1999); while in the lower part

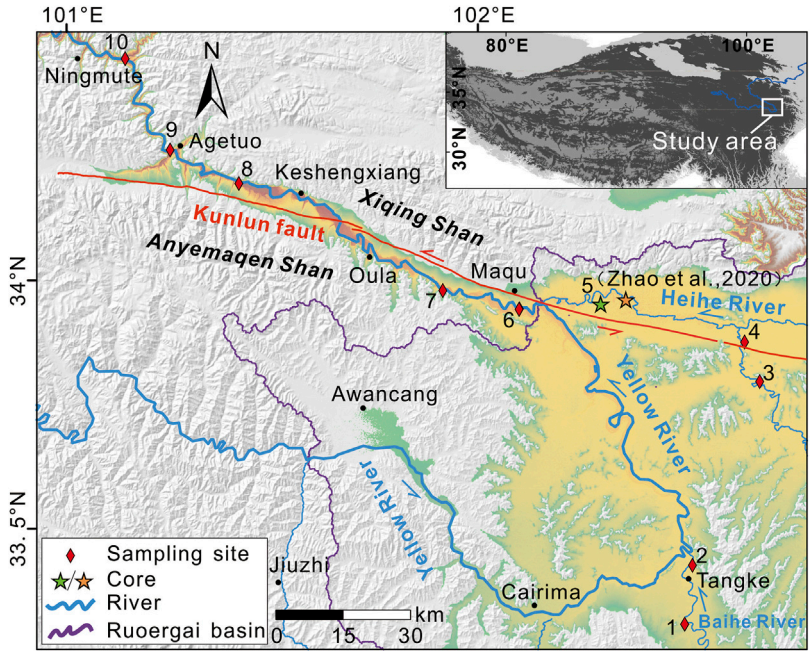

FIGURE 1
The study area and the source of the Yellow River shown in Google Earth and DEM images. Numbers 1–10 denote the sampling sites. The green star represents the core sampling site of this study, and the orange star represents the core sampling site of Zhao et al. (2020).

(108–116 m) of the RH core, the coarse sand and fine gravel layers have evolved (Wu et al., 1997). Based on the drilling results (at a depth of about 150 m) and magnetotelluric investigations, the Sichuan Geological Survey Institute (2008) stated that a paleo-paternoster lake was present in the Ruoergai Basin, and the paleolake sediment is covered by a fluvial gravel layer of more than 200 m. The sedimentary center of the basin is located in the downstream area of the Heihe River in the north of the basin, and the paleolake area is gradually shrinking (Sheng et al., 2007). Currently, the Huahu area in the northeast of the basin still has a lake environment. Li et al. (2016) summarized the upper sediments of the Ruoergai Basin, established the stratigraphic sequence of the basin since the middle of late Pleistocene (75 ka), divided it into six sedimentary rhythms from the bottom to the top, and considered that the sedimentary process was mostly influenced by climate change. Recently, we drilled through the Quaternary sediments in the Yellow River belt on the west side of the Ruoergai Basin and found alluvial sandstone and gravel beds with a thickness of more than 200 m. According to preliminary dating results, the optically stimulated luminescence (OSL) age at the top 50 m is more than 70 ka (Institute of Geology and China Earthquake Administration and Sichuan Geological Engineering Exploration Institute Group Co, Forthcoming 2022). The drilling data in the deep and shallow areas presented above signify that the Ruoergai Basin is more than just a single lake–river transition event on the surface and it may have undergone a more complex evolution process of paleolake, river–lake coexistence, and river dominance.

The Yellow River flows out from the northwest corner of the Ruoergai Basin, flowing through the Maqu wide valley formed by the piedmont proluvial fan groups sandwiched between the Xiqing Shan and Anyemaqen Shan and then enters the bedrock gorge area after cutting into the mountains on the west side of the Xiqing Shan from Agetuo. In this study, the Cairima–Ningmute reach, which includes the basin, wide valley, and gorge landforms shown in Figure 1, is denoted as the outlet reach of the Yellow River in the Ruoergai Basin. Strong geological agents exist both inside and outside the reach, such as the activity of the East Kunlun fault and the development of the Quaternary glacier in the Anyemaqen Shan. At the basin-canyon bottleneck, the substantial accumulation of large amounts of coarse debris from both sides of the Maqu Valley may lead to the blockage of the Yellow River channel and the formation of dammed lakes (Zhao et al., 2019). In the alpine gorge areas of the eastern and southern edges of the Qinghai–Tibet Plateau, damming events frequently occur and play an important role in the evolution of river geomorphology (Ouimet et al., 2007; Zhao et al., 2015; Wu et al., 2016; Hu et al., 2018, 2020; Liu et al., 2019). For example, research on the Yarlung Tsangpo River grand canyon in the southeastern region of the Tibetan Plateau indicates that repeated glacial dams blocking the river at the grand canyon's entrance prevent the river from flowing down to the interior of the Tibetan Plateau and that the blocking of the river storage may cause numerous catastrophic glacial outburst floods through the Yarlung Tsangpo River grand canyon, which may be the main cause for the rapid cutting of the Quaternary Yarlung Tsangpo bend (Korup and Montgomery, 2008; Lang et al., 2013).

In this study, we conduct a field survey and sample dating based on the geomorphic and sedimentary characteristics of the outlet reach of the Yellow River in the Ruoergai Basin, with surface terraces as the main research object. Moreover, we use the dam-barrier model to interpret the geomorphic evolution process and driving mechanism of the Yellow River outlet section in the Ruoerge Basin during the late Quaternary.

2 Regional settings

The study area is mainly located at the end of the east Kunlun Fault Zone, which is an important late Quaternary left-slip fault in the northeastern part of the Tibetan Plateau with NWW direction and dip-slip component. The fault cuts across the Yellow River's source region and spans the Anyemaqen Shan, which has a high terrain and an average elevation of roughly 4,500 m. The eastern section of the fault extends along the northern edge of the Maqu valley–Ruoergai Basin, comprises the Heihe River, and extends out of the swamp present north of the Ruoergai Basin (Figure 1). The climate in the study area is mainly cold and humid, with typical plateau continental climate characteristics, the annual average temperature ranges between −5.6°C and 3.8°C, and the annual average precipitation ranges between 260 and 610 mm (Chen et al., 2017). Moreover, approximately 70%–75% of the annual precipitation falls between June and September and is frequently accompanied by small-scale natural disasters, such as landslides and debris flows. The annual evaporation ranges from 700 to 1,500 mm.

The Yellow River flows from the northwest corner of the Ruoergai basin with considerable sediments and enters the wide valley of Maqu, which is composed of piedmont proluvial fans sandwiched between the Xiqing Shan and Anyemaqen Shan, gradually transitioning from sedimentation to erosion (Harkins et al., 2007). Then, it cuts into the western piedmont of the Xiqing Shan from the Agetuo and turns into bedrock. The corresponding river terrace also gradually transitions from accumulation terrace to erosion terrace (Kirby et al., 2007). Due to the comprehensive influence of the geological structure, fault activity, bedrock lithology, glacier, and other elements in the research area, the valley geomorphology and sedimentation exhibit noticeable segmentation (Supplementary Figure S1). The valley can be divided into three sections, and the geomorphological features of each section are shown as follows.

2.1 Cairima–Maqu

The reach is located in the Ruoergai Basin, with a total length of ~155 km, an elevation range of 3,410–3,380 m, a drop of 30 m, and an average slope of 0.19‰. The region includes meandering rivers and oxbow lakes, and the reach is "I" shaped. A Holocene peat layer generally developed in this reach, and the sedimentary thickness ranges from 0.5 to 10 m, such as the famous peat swamp sediments in the lower reaches of the Baihe River (Supplementary Figure S2A). The river surface abruptly widens at the confluence of the Heihe River and Yellow River. The basins are primarily small alluvial plains on both sides of the Heihe River (Supplementary Figure S2B), which have developed into 1–2 river terraces (Supplementary Figure S2C) due to poor vegetation in the study area, frequent aeolian activities, and aeolian accumulation in the form of surface sand dunes (Supplementary Figure S2D).

2.2 Maqu–Agetuo

The reach is located in the middle section from the outlet of the Ruoergai Basin to the canyon area, where the Yellow River flows between the Anyemaqen Shan and Xiqing Shan. The reach is approximately 110 km long, with an elevation range of 3,380–3,280 m, a 100-m plunge, an average longitudinal gradient of 0.91°, and a broad U-shaped river valley (Supplementary Figure S3C). The width is typically 200–500 m, with an average valley width of 350 m. The river reach mainly comprises 3–5 levels of river terraces, with the terrace-type gradually transitioning from accumulation terrace to bedrock terrace. The complex, diverse, widely dispersed, and thickly sedimentary Quaternary overburden in this river stretch is mostly composed of alluvium, flood sedimentation, fluvial accumulation, and glacial mixed buildup (Supplementary Figure S3D). Alluvial ditches have developed on both sides of the river valley, and fan-shaped accumulations are present at the mouth of branch trench (Supplementary Figure S3A). Flood sediments are mainly distributed on the left bank of the river in the Maqu–Oula section. Due to the high temperatures in the summer, the melting of glaciers on the Anyemaqen Shan will afford residual freeze–thaw structures in the local areas on the surface (Supplementary Figure S3B) and the drainage of meltwater will cause regional seasonal flooding.

2.3 Agetuo–Ningmute

The reach is located between the canyon entrance and Ningmute (Supplementary Figure S4A). Its channel's longitudinal gradient is around 11.58, making it a "V"-shaped valley (Supplementary Figure S4B). The lower valley slope is steep, with a slope angle of 60°–90°. The valley in the bedrock canyon area has been cut down to ~90 m, and bedrock terrace has developed on both sides of the valley.

3 Methodology

3.1 Field surveying and sampling

Major Quaternary sediments, such as fluvial-lacustrine sediments and outburst flood sediments, as well as major geomorphological types, such as moraine monuments, fluvial terraces, and flood terraces, have been identified in the field. In this study, high-resolution Google Earth images and 90-m resolution elevation data from the Shuttle Radar Topography Mission (https://www2.jpl.nasa.gov/srtm/) were used to identify the boundaries of the geomorphic types in the study area. The elevation, relative distance, and other basic information of different landforms in real-time differential correction were measured using the Global Satellite System receiver (Trimble Juno3E). Furthermore, the sediments were sampled for OSL dating by hammering stainless steel tubes into a natural sediment profile, and the sample depths were determined using a tape measure. The filled stainless steel tubes were removed from the sediments and immediately wrapped with an aluminum foil and tape to avoid exposure to sunlight during transportation. Samples of organic materials for ^{14}C dating were selected from the core library and stored in sealed plastic bags.

3.2 Dating

3.2.1 Optically stimulated luminescence dating

In this study, a total of 27 OSL samples were measured at the Laboratory of Luminescence dating, State Key Laboratory of Earthquake Dynamics, Institute of Geology, China Earthquake Administration. The samples were extracted from the inner part of the tubes and quartz was purified using conventional sample preparation techniques (dissolving carbonates with 10% HCl, oxidizing organic matter with 10% H_2O_2, settling using Stokes' Law, dissolving feldspars by 30% fluorosilicic acid, followed by immersion in 10% HCl) for the 4–11 μm fine grain quartz (FQ) fraction (Aitken, 1998; Liu et al., 2010), and 90–250 μm coarse grain quartz (CQ) fractions (sieving, 10% HCl, 10% H_2O_2, etching with 40% HF, followed by immersion in 10% HCl). The purity of the quartz extracts was confirmed by the absence of an IRSL signal for both FQ and CQ. Subsamples of FQ had IR signals close to background levels, with an IR-OSL depletion ratio between 0.9 and 1.1. Nevertheless, an IR-OSL depletion test (Duller, 2003) was carried out on every aliquot for small aliquot CQ. All the De values of samples were measured on a Risø TL/OSL Reader model DA-20 equipped with a calibrated 90Sr/90Y beta radiation source (dose rate 0.1125 Gy/s for CQ and 0.1045 Gy/s for FQ in the standard configuration), blue

TABLE 1 OSL dating results of sediments in the Caiyima-Ningmut section of the Yellow River source.

Sample no.	Depth (m)	Grain size (μm)	Aliquots[a]	U (ppm)	Th (ppm)	K (%)	Water content (%)	Od (%)	Dose rate (Ga/ka)	De[b] (Gy)	Age (ka)	References
Site 1, 33°19′2.98″N, 102°27′13.32″E, 3,439 m asl												
CEQ19-1	1.00	4–11	12	1.30 ± 0.32	8.35 ± 0.26	1.26 ± 0.04	10 ± 5	N/A	2.7 ± 0.2	24.7 ± 1.6	9.2 ± 0.8	This study
CEQ19-2	1.95	4–11	12	1.91 ± 0.25	11.88 ± 0.22	1.92 ± 0.03	10 ± 5	N/A	3.8 ± 0.2	40.6 ± 1.4	10.7 ± 0.7	This study
CEQ19-3	2.90	4–11	12	2.06 ± 0.05	13.84 ± 0.24	2.08 ± 0.03	10 ± 5	N/A	4.1 ± 0.2	76.7 ± 4.2	18.5 ± 1.5	This study
Site 2, 33°26′7.63″N, 102°9′28.10″E, 3,421 m asl												
FJC19-1	2.00	4–11	12	1.86 ± 0.43	7.64 ± 0.56	1.40 ± 0.03	10 ± 5	N/A	2.9 ± 0.2	1.7 ± 0.1	0.6 ± 0.1	This study
Site 3, 33°52′51.80″N, 102°37′15.90″E, 3,423 m asl												
KSE19-1	1.50	4–11	12	1.60 ± 0.06	10.43 ± 0.42	1.68 ± 0.06	10 ± 5	N/A	3.4 ± 0.2	32.2 ± 1.4	9.6 ± 0.6	This study
KSE19-4	4.30	4–11	12	1.44 ± 0.07	8.13 ± 0.31	1.36 ± 0.02	10 ± 5	N/A	2.7 ± 0.2	25.2 ± 3.6	9.4 ± 1.5	This study
Site 4, 33°48′2.55″N, 102°39′12.82″E, 3,427 m asl												
ZC19-1	2.90	4–11	12	1.40 ± 0.11	8.76 ± 0.26	1.53 ± 0.02	10 ± 5	N/A	2.9 ± 0.2	33.2 ± 3.3	10.9 ± 1.3	This study
ZC19-2	3.80	4–11	12	1.37 ± 0.09	8.02 ± 0.53	1.43 ± 0.04	10 ± 5	N/A	2.7 ± 0.2	32.5 ± 1.9	11.9 ± 1.0	This study
ZC19-3	5.60	4–11	12	1.87 ± 0.13	7.64 ± 0.17	1.4 ± 0.04	10 ± 5	N/A	2.8 ± 0.2	26.0 ± 1.6	9.3 ± 0.8	This study
Site 5, 33°58′1.03″N, 102°16′35.93″E, 3,424 m asl												
ZK3-02	0.80	90–180	20/48	1.90 ± 0.59	8.20 ± 0.20	1.35 ± 0.05	10 ± 5	19	2.4 ± 0.1	25.7 ± 1.5	10.8 ± 0.9	This study
ZK3-05	3.50	90–180	29/48	2.60 ± 0.65	3.00 ± 0.06	1.48 ± 0.05	10 ± 5	14	2.5 ± 0.1	21.6 ± 0.8	8.6 ± 0.6	This study
ZK3-07	6.90	90–180	21/48	1.30 ± 0.50	7.40 ± 0.20	1.35 ± 0.05	10 ± 5	8	2.1 ± 0.1	18.7 ± 0.8	9.1 ± 0.7	This study
ZK3-14	15.40	90–180	35/48	2.40 ± 0.73	12.70 ± 0.30	1.62 ± 0.06	10 ± 5	21	2.8 ± 0.2	87.2 ± 6.9	31.7 ± 3.2	This study
Site 6, 33°57′45.17″N, 102°4′50.69″E, 3,428 m asl												
MQQ19-1	4.40	4–11	12	1.95 ± 0.08	9.61 ± 0.22	1.60 ± 0.05	10 ± 5	N/A	3.2 ± 0.2	38.9 ± 1.7	12.0 ± 0.9	This study
MQQ19-3	4.00	150–180	12/42	1.81 ± 0.22	9.35 ± 0.16	1.40 ± 0.05	10 ± 5	61	2.4 ± 0.1	15.1 ± 4.8	6.3 ± 2.0	This study
MQQ19-9	1.70	90–125	24/42	1.23 ± 0.17	6.28 ± 0.18	1.26 ± 0.03	10 ± 5	6	2.1 ± 0.1	3.0 ± 0.2	1.4 ± 0.1	This study
MQQ19-10	0.03	4–11	12	1.81 ± 0.66	9.76 ± 0.23	1.61 ± 0.03	10 ± 5	N/A	3.5 ± 0.2	0.7 ± 0.1	0.2 ± 0.1	This study
Site 7, 34°00′14.76″N, 101°53′49.93″E, 3,410 m asl												
MR19-1	13.30	150–180	21/42	1.16 ± 0.27	5.93 ± 0.37	1.43 ± 0.02	10 ± 5	14	1.9 ± 0.1	104.4 ± 4.0	53.7 ± 4.1	This study
MR19-2	11.80	90–125	23/42	1.83 ± 0.33	10.43 ± 0.64	1.60 ± 0.06	10 ± 5	16	2.6 ± 0.2	115.6 ± 4.3	44.9 ± 3.3	This study
MR19-3	2.70	4–11	12	1.71 ± 0.20	10.48 ± 0.22	1.84 ± 0.07	10 ± 5	N/A	3.5 ± 0.2	56.0 ± 2.5	16.1 ± 1.2	This study
MR19-4	7.10	125–150	18/42	1.39 ± 0.35	7.40 ± 0.18	1.25 ± 0.05	10 ± 5	15	2.0 ± 0.1	49.2 ± 2.0	24.6 ± 1.9	This study
Site 8, 34°13′47.84″N, 101°24′36.29″E, 3,395 m asl												
HHLS19-1	3.50	4–11	12	3.28 ± 0.06	13.19 ± 0.16	2.05 ± 0.04	10 ± 5	N/A	4.6 ± 0.3	226.8 ± 15.8	50.9 ± 4.7	This study

(Continued on following page)

TABLE 1 (*Continued*) OSL dating results of sediments in the Caiyima-Ningmut section of the Yellow River source.

Sample no.	Depth (m)	Grain size (μm)	Aliquots[a]	U (ppm)	Th (ppm)	K (%)	Water content (%)	Od (%)	Dose rate (Ga/ka)	De[b] (Gy)	Age (ka)	References
Site 9, 34°18′3.76″N, 101°14′42.84″E, 3,391 m asl												
CYD20-1	2.40	90–180	22/48	2.40 ± 0.65	3.50 ± 0.07	1.67 ± 0.06	10 ± 5	10	2.6 ± 0.2	58.3 ± 7.8	22.1 ± 3.2	This study
CYD20-2	2.00	90–180	26/48	2.40 ± 0.59	3.00 ± 0.06	1.43 ± 0.05	10 ± 5	10	2.5 ± 0.2	61.2 ± 10.0	26.7 ± 4.6	This study
CYD20-4	2.70	90–180	21/48	1.06 ± 0.06	2.80 ± 0.06	1.31 ± 0.04	10 ± 5	10	2.5 ± 0.1	53.1 ± 8.8	21.5 ± 3.8	This study
Site 10, 34°29′7.92″N, 101°8′34.24″E, 3,347 m asl												
NMT19-1	4.00	90–125	30/72	2.00 ± 0.48	8.30 ± 0.17	1.25 ± 0.04	10 ± 5	27	2.2 ± 0.1	28.3 ± 2.9	12.9 ± 1.5	This study
NMT19-2	3.20	90–125	48/72	2.20 ± 0.48	8.30 ± 0.17	1.25 ± 0.04	10 ± 5	36	2.3 ± 0.1	30.8 ± 3.4	13.7 ± 1.7	This study
TWR-OSL-01	0.28–0.29	N/A	N/A	2.24 ± 0.09	10.9 ± 0.31	1.86 ± 0.06	10	N/A	3.05 ± 0.18	39.61 ± 2.34	12.98 ± 1.09	Chen et al. (2017)
TWR-OSL-02	0.41–0.42	N/A	N/A	2.41 ± 0.10	10.8 ± 0.30	1.75 ± 0.06	10	N/A	3.25 ± 0.19	41.49 ± 2.69	13.59 ± 1.2	Chen et al. (2017)
Section 1–02	1.20	N/A	N/A	1.62 ± 0.21	6.68 ± 0.36	1.40 ± 0.08	N/A	N/A	2.47 ± 0.18	25.36 ± 0.72	10.27 ± 0.81	Hu et al. (2018)
KSXDM-OSL-170	N/A	N/A	13	1.86 ± 0.09	10.18 ± 0.51	1.75 ± 0.04	5.5	N/A	3.06 ± 0.08	36.51 ± 1.94	11.9 ± 0.7	Liu et al. (2021)
OL-OSL-350	N/A	N/A	13	1.47 ± 0.07	7.82 ± 0.39	1.55 ± 0.03	9.6	N/A	2.46 ± 0.1	34.83 ± 1.86	14.1 ± 0.9	Liu et al. (2021)
MQ2-OSL-620	N/A	N/A	12	1.35 ± 0.07	7.07 ± 0.35	1.43 ± 0.03	1.7	N/A	2.12 ± 0.03	27.46 ± 1.21	12.9 ± 0.6	Liu et al. (2021)
OL-OSL-200	N/A	N/A	14	1.72 ± 0.09	9.49 ± 0.47	1.63 ± 0.03	7	N/A	2.81 ± 0.09	33.97 ± 2.34	12.1 ± 0.9	Liu et al. (2021)
MQ2-OSL-120	N/A	N/A	11	1.43 ± 0.07	7.43 ± 0.37	1.42 ± 0.03	2.5	N/A	2.56 ± 0.05	3.4 ± 0.59	1.3 ± 0.3	Liu et al. (2021)
KSXDM-OSL-300	N/A	N/A	15	1.35 ± 0.07	7.07 ± 0.35	1.43 ± 0.03	1.7	N/A	2.12 ± 0.03	36.51 ± 1.94	4.2 ± 0.3	Liu et al. (2021)

[a]The value on the left represents the number of only valid pieces, and the value on the right represents the total number of pieces. The Simple-aliquot Regenerative Dose (SMAR) protocol was used for equivalent dose (De) determination of fine particles (4~11 μm) quartz samples, where 12 slices were measured for each sample, 6 natural slices and 6 regenerative dose point slices.

[b]With the exception of samples MQQ19-3, ZK3-14, NMT19-1, and NMT19-2, for which the equivalent dose D_e was calculated using the minimum value model, the equivalent dose D_e for coarse-grained (>90 μm) and fine-grained (4–11 μm) quartz was calculated using the central value model and the mean value, respectively (Galbraith, 2010).

(470 ± 30 nm; ~50 mW/cm^2) and infrared (880 ± 40 nm, ~145 mW/cm^2) light sources, and detection through a 7-mm thick U-340 glass filter.

The Simple-aliquot Regenerative Dose (SMAR) protocol and Simple Multiple Aliquot Regenerative Dose (SA-SGC) protocol were used for equivalent dose (De) determination of fine particles (4~11 μm) quartz samples (Lu et al., 2007) and coarse grain quartz (Faershtein et al., 2016; Yang et al., 2017) respectively. The preheat and cut-heat temperatures were respectively 240°C and 200°C (Fan, 2021).

The U, Th, and K contents were measured by inductively coupled plasma mass spectrometer, and the values are given in Table 1. All the samples are above groundwater level and the water content was assumed to be 10% ± 5% (Chen et al., 2017). The dose rate for each sample is calculated directly by using the observed radionuclide concentrations and attenuation values from Aitken (1998). Besides, the water content of the sample and cosmic ray contribution, as well as alpha efficiency value were considered for accurate calculation of the environmental dose (Prescott and Hutton, 1994; Rees-Jones, 1995; Lai et al., 2008).

3.2.2 14C dating

The six ^{14}C samples collected in this study were mainly carbon and plant debris from lacustrine sedimentary layers in the Ruoergai core (ZK03), and all samples were analyzed at the

TABLE 2 AMS-^{14}C dating of shallow sediments from the Ruoergai core.

Sample ID	Material	Depth (m)	^{14}C age (yr BP)	Calibrated^{14}C age (ka BP)	References
ZK3-14C-1	Charcoal	5.1	14,870 ± 60	18.088 ± 0.191	This study
ZK3-^{14}C-5	Plant remains	6.7	12,260 ± 40	14.149 ± 0.150	This study
ZK3-^{14}C-6	Charcoal	7.9	10,490 ± 30	12.489 ± 0.079	This study
ZK3-^{14}C-3	Charcoal	9.5	34,480 ± 250	39.040 ± 0.565	This study
ZK3-^{14}C-2	Charcoal	10.54	31,520 ± 180	35.401 ± 0.461	This study
ZK3-^{14}C-4	Charcoal	13.48	40,180 ± 420	43.811 ± 0.769	This study
Beta-448696	Sedge leaves	5.63	6,320	7.243 ± 0.068	Zhao et al. (2020)
Beta-395809	Sedge leaves+Phragmites leave	7.45	15,610	18.853 ± 0.083	Zhao et al. (2020)

Beta Laboratory for Analytical Radiocarbon Dating in the US. The samples were prepared and tested using gas pedal mass spectrometer (AMS) radiocarbon dating. Firstly, the samples were first sieved using a 180 μm sieve, the organic sediments were pretreated with acid washing to remove carbonates, while the carbon chip samples were pretreated using the acid–base washing method. Finally, the radiocarbon ages of all the ^{14}C samples were corrected to calendar years using the Calib Rev 8.2 programs of the IntCal 20 calibration curve (Stuiver et al., 2020), and the age results are listed in Table 2.

3.1.3 Reliability of dating results

The accuracy of the results of the fluvial and lacustrine sediment dating may be affected by the partial bleaching of sediment OSL signals (Zhang et al., 2003; Hu et al., 2018, 2020). The distribution of the *De* values can be used to access the OSL signals, and Figure 2 displays the representative luminescence dose growth curves of the coarse and fine quartz grains as well as a linear distribution diagram of the *De* value of the coarse quartz grains. This *De* distribution is approximately normal (Figure 2A), denoting that most of the samples were fully weathered before burial (Zhang et al., 2003; Arnold et al., 2009; Thrasher et al., 2009a; Thrasher et al., 2009b). However, two peaks are clearly present in the *De* distribution curves of several samples (ZK3-2, ZK3-7, ZK3-14, MQQ19-9, MR19-1, and CY020-1). The ZK3-2 sample was taken as an example (Figure 2B); it was collected at the drilling depth of 0.8 m. Its OSL age was 10.8 ± 0.9 ka (Table 1; Supplementary Figure S6), while the OSL age of the ZK3-5 sample collected at a depth of 3.5 m was 8.6 ± 0.6 ka (Table 1; Supplementary Figure S6). The OSL age of the ZK3-2 sample was determined using the central age model, and the result was obviously overestimated, indicating that the sample was not fully bleached before burial. Therefore, we consider that the age of 10.8 ± 0.9 ka may be an outlier. Two samples, denoted as KSE19-1 and KSE19-4, were taken from the same section (Supplementary Figure S5C) with ages of 9.6 ± 0.6 and 9.4 ± 1.5 ka (Table 1), respectively, and the light release dose growth curves and signal decay curves of their fine-grained quartz are shown in Figures 3C,D. Although inverted, the two ages are reliable within the margin of error; this feature was shared by two other samples, denoted as NMT19-1 and NMT19-2, which were taken from the same section (Supplementary Figure S9B) with ages of 13.7 ± 1.7 and 12.9 ± 1.5 ka (Table 1), respectively. Based on all the evidence, most OSL ages are assumed to be reliable and to represent the burial time of the sediments.

4 Results

4.1 Dammed lake

To study the evolutionary history of the river in the Ruoergai outlet section, numerous field surveys were conducted. We found that the Ruoergai Basin mainly comprises dammed lake sedimentation, with lake sediments as the base and 1–2 river terraces, and the terraces mainly contain fine grain sediments. The reach from Maqu to Agetuo mainly comprises barrier dam sedimentation, with mostly coarse-grained clastic sediments. It has developed into U-shaped valleys, transitioning from accumulation terraces to base terraces; the lower reach of Agetuo has developed into a canyon area and has developed bedrock terrace, constituting the sedimentary system of paleo-damming. In this study, nine typical sites and one drilling core were adopted for geomorphological and sedimentary geological analysis.

The valleys of the Baihe River and Heihe River in the Ruoergai Basin are narrow; they are mainly braided rivers and comprise side beaches, channel bars, and oxbow lakes. The lacustrine sediments are mainly exposed on the T2 terrace in the river section of the Tangke Township, which is often interlayered with river sand layers to form a river–lake sedimentary cycle and constitute a lacustrine terrace (Figure 3).

4.1.1 Baihe River terrace

Site 1 is located in the upper reaches of the White River near Tangke town (Figure 1), where the valley is ~0.2 km wide and

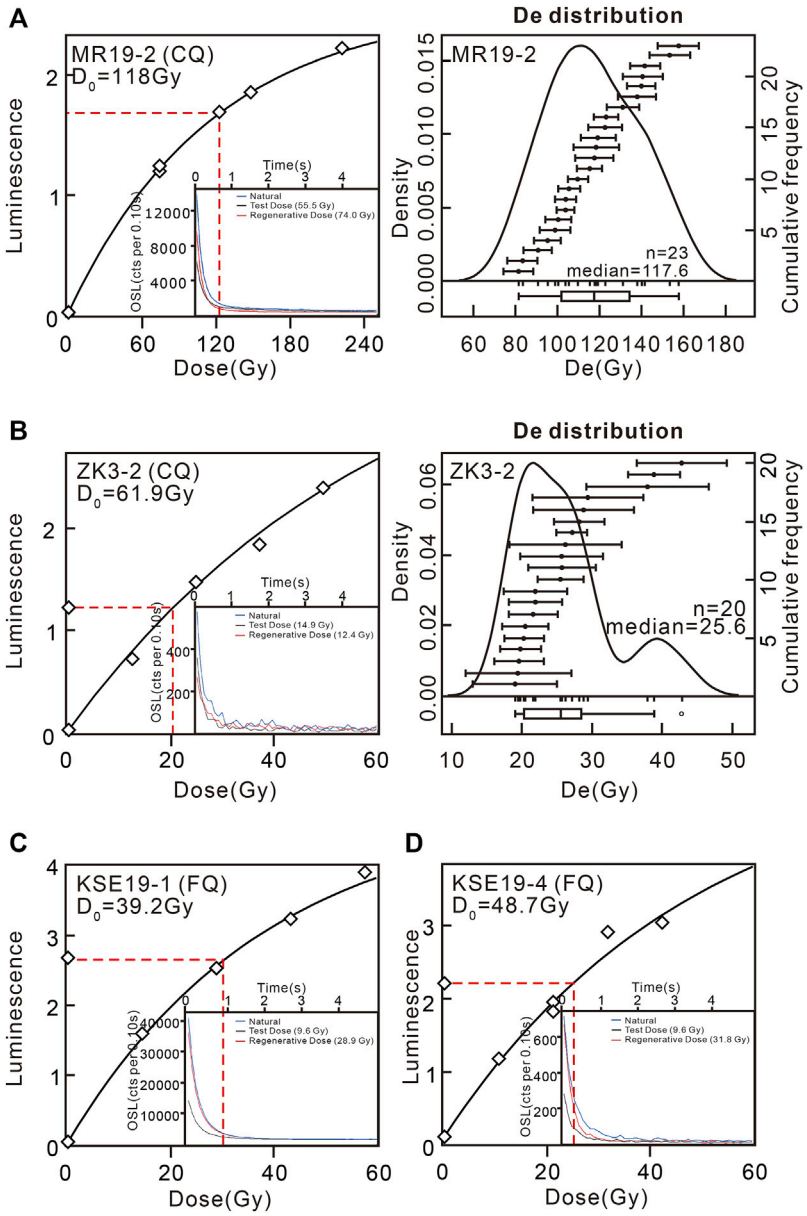

FIGURE 2
Curve plots showing the dose growth, shine down curves (inset) for sample MR19-2, ZK3-2, KSE19-1, and KSE19-4 and dose distribution for sample MR19-2, ZK3-2.

mainly has T1 and T2 terraces (Figure 3A). The sampling section profile is 5.7 m thick; the upper part comprises a 0.4-m-thick black humus layer and the middle part comprises a 2-m-thick gray-white clayey chalk layer with yellow-brown stripes. Two OSL samples CEQ19-1 and CEQ19-2 were buried at 1 and 1.95 m depths in the middle layer, respectively. The lower part is composed of 3.3-m-thick greenish gray clay with lacustrine sedimentation, where the CEQ19-3 OSL sample was taken at the depth of 2.9 m (Supplementary Figure S5A).

Site 2 is located near Tangke town (Figure 1), and it is mainly situated in the T1 terrace on the east bank of the Baihe River (Figure 3A). The total height of the profile is 5 m, consisting of three sets of strata. The uppermost strata are a 1-m-thick soil layer; the middle strata are a 2-m-thick gray-yellow fine sand layer, where the FJC19-1 OSL sample was extracted at the depth of 2 m; and the lowermost strata are a 2-m-thick yellow coarse sand layer (Supplementary Figure S5B).

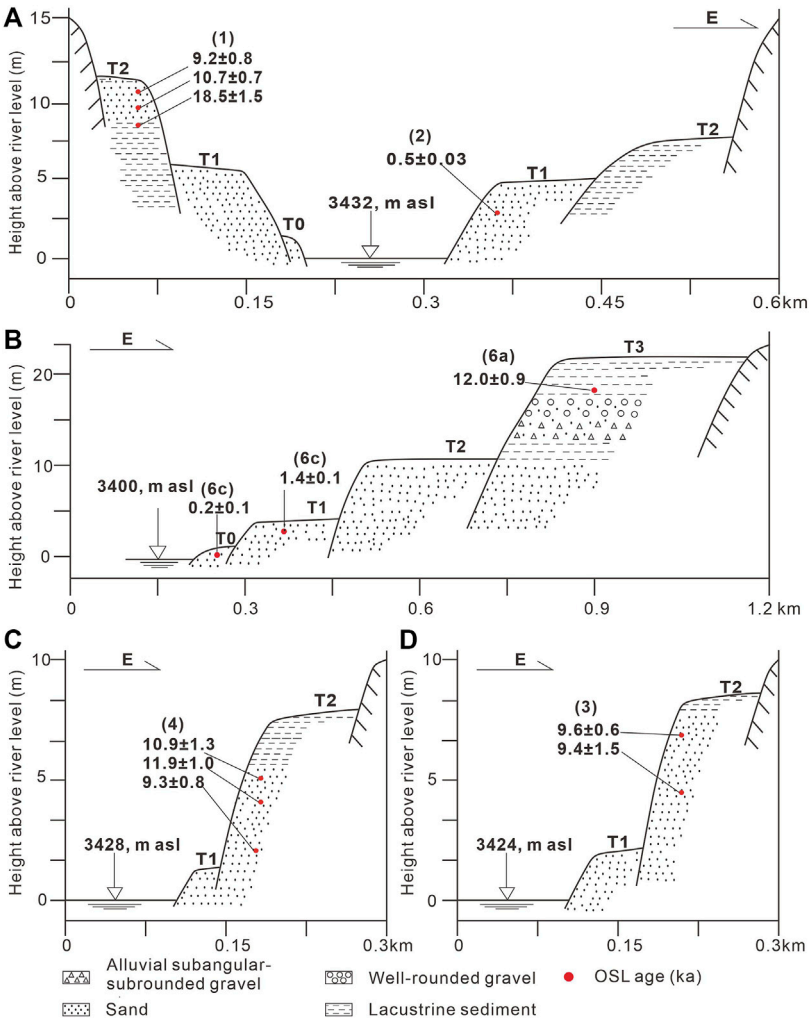

FIGURE 3
Schematic transverse sections of the terraces (sites 1–4 and 6), with dating data.

4.1.2 Heihe River terrace

Sites 3 and 4 are located in the middle reach of the Heihe River (Figures 3C,D), and the profiles of both are fluvial sand sedimentation of silty sand interbedded with medium sand. As shown in Supplementary Figure S5C, the profile has a total height of 6.3 m and comprises two sets of strata. The upper part is a 0.9-m-thick black-brown topsoil layer and the lower part is a fluvial sand layer of greenish gray fine chalk sand interbedded with yellow-brown fine and medium sand, where the KSE19-1 and KSE19-4 OSL samples were extracted at depths of 1.5 and 4.3 m, respectively.

The sampling profile near the sampling site 4 has a total height of 6 m and comprises three sets of strata. The uppermost strata are a 1.6-m-thick topsoil layer containing plant roots, the middle strata are a 0.9-m-thick yellow-brown clay layer, and the lowermost strata are a river sand layer of greenish gray silty sand interbedded with yellow medium sand, where the ZC19-1, ZC19-2, and ZC19-3 OSL samples were taken at the depths of 2.9, 3.8, and 5.6 m, respectively.

Toward the downstream direction, typical lacustrine strata are present on both sides of the river valley, and the lacustrine sediments are relatively thick. A deep drilling (Site 5) was established on the flat geomorphological surface of the T2 terrace near the Zexiu Village downstream of the Heihe River. The 25 m core from the top of the drilling denotes the last fluvio-lacustrine facies transition of the Ruoergai Basin (Supplementary Figure S6A), and the specific descriptions and sampling locations are as follows:

(1) 0–8 m: Fluvial sediments - The upper section is steel-gray fine silty sand with a thickness of ~40 cm, and plant root system can be seen in it. The middle section mainly

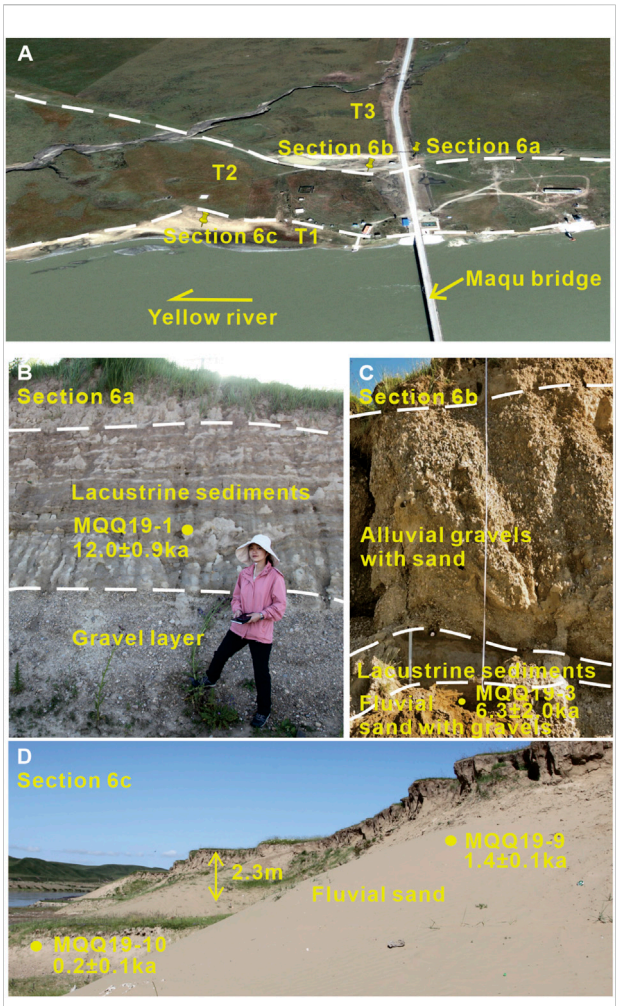

FIGURE 4
(A) Google Earth image showing the terraces near the Maqu Bridge. **(B)** Photograph showing the sedimentary properties of Section 6a, with OSL age. (Author shown in image) **(C)** Photograph showing the sedimentary properties of Section 6b, with OSL age. **(D)** Photograph showing the sedimentary properties of Section 6c, Q20 with OSL ages.

comprises a layer of yellowish brown fine sand with a thickness of ~4.5 m, and oblique bedding can be seen in it. Two OSL samples were taken at depths of 0.8 and 3.5 m, respectively. Brown-yellow silt of fluvial facies and light gray muddy silt are interbedded 3 m away from the lower section, and parallel bedding is present. Three ^{14}C samples were taken at the depths of 5.1, 6.7, and 7.9 m, and one OSL sample was taken at a depth of 6.9 m.

(2) 8–16 m: Lacustrine sedimentation - It is mainly composed of gray argillaceous silt sediment, and pinnate cross-bedding is obviously present from a depth of 13.8 m, and three ^{14}C samples were taken at depths of 9.5, 10.54, and 13.48 m.

(3) 16–25 m: Flood plain sedimentation - It is mainly composed of grayish black compact clay of alluvial facies and lacustrine facies and yellowish gray muddy silt of alluvial swamp facies, and it is interbedded with several layers of grayish black silty mud sediments.

4.1.3 Maqu bridge terrace

Site 6 is located near the Maqu bridge, about 10 km from the outlet of the Ruoergai Basin; it is mainly composed of three fluvial terraces (Figures 3B, 4A). The height of the terraces are ~5, ~12, and ~20 m. The T1 and T2 terraces are fluvial sedimentary terraces, and lake sediments are preserved in the T3 terrace. T0 and T1 terraces comprise brownish-yellow coarse sand sediments of the river floodplain (Figure 4D). Two OSL samples (MQQ19-10 and MQQ19-9) were taken at depths of 0.3 and 1.7 m, respectively. The T2 terrace has an exposed ~5.5 m yellow-brown medium-fine sandy sedimentary profile, and the OSL sample MQQ19-8 was taken at a depth of 1.4 m. The T3 terrace has two sampling profiles. One is located at the roadside (Figure 4B) and ~8.5 m is exposed. The upper part is a 1.5-m-thick light yellow clay layer, and the middle part is a 4-m-thick yellow fine sand layer and gray-brown mud interlayers with clear lacustrine sediments, and OSL sample MQQ19-1 was collected at a depth of 4.4 m. The lower part is a 3 m gravel layer; the roundness of the gravel is not good, with an average grain size of 2–5 cm. The lithology is mainly composed of limestone, sandstone, and schist and contains a small amount of vein quartz and calcite. The gravel contains grayish yellow silt lens. About 4.1 m of the other profile is exposed (Figure 4C), with a 0.4-m-thick topsoil layer in the upper part, a 2-m-thick gray-white sand and gravel layer in the middle, which is interspersed with gray-white fine sand lenses, and a 0.5-m-thick gray-white clayey sand layer in the lower part, corresponding to the lake phase layer in the first T3 profile. A yellow fine sand layer is present further down, and the MQQ19-3 an OSL sample was collected at the depth of 4 m.

The ages of the 11 fluvial sedimentation samples taken from the fluvial terraces within the Ruoergai Basin and near the outlet of Maqu range from 0.2 to 11.9 ka, which is consistent with the results of previous studies conducted in this basin (Table 1). According to the ages of the ZK3-5 and ZK3-14C-5 samples, which were taken at depths of 3.5 and 6.7 m, respectively, the sedimentary rate of the fluvial facies is determined to be 0.5 mm/a (Supplementary Figure S6C), which is approximately consistent with the Bayesian age model established by Zhao et al. (2020) through the sample age of 10 m at the top of the core (ZB13-C2: 33°58.163′N, 102°19.855′E, 3,434 m above sea level; Figure 1). The boundary of the transition from fluvio-lacustrine facies to terrace facies in the Ruoergai Basin is ~12 ka.

The age of the OSL sample from the lacustrine sedimentary part of site 1 was 18.5 ± 1.5 ka, and the age of the OSL sample from the lacustrine sedimentary layer of the

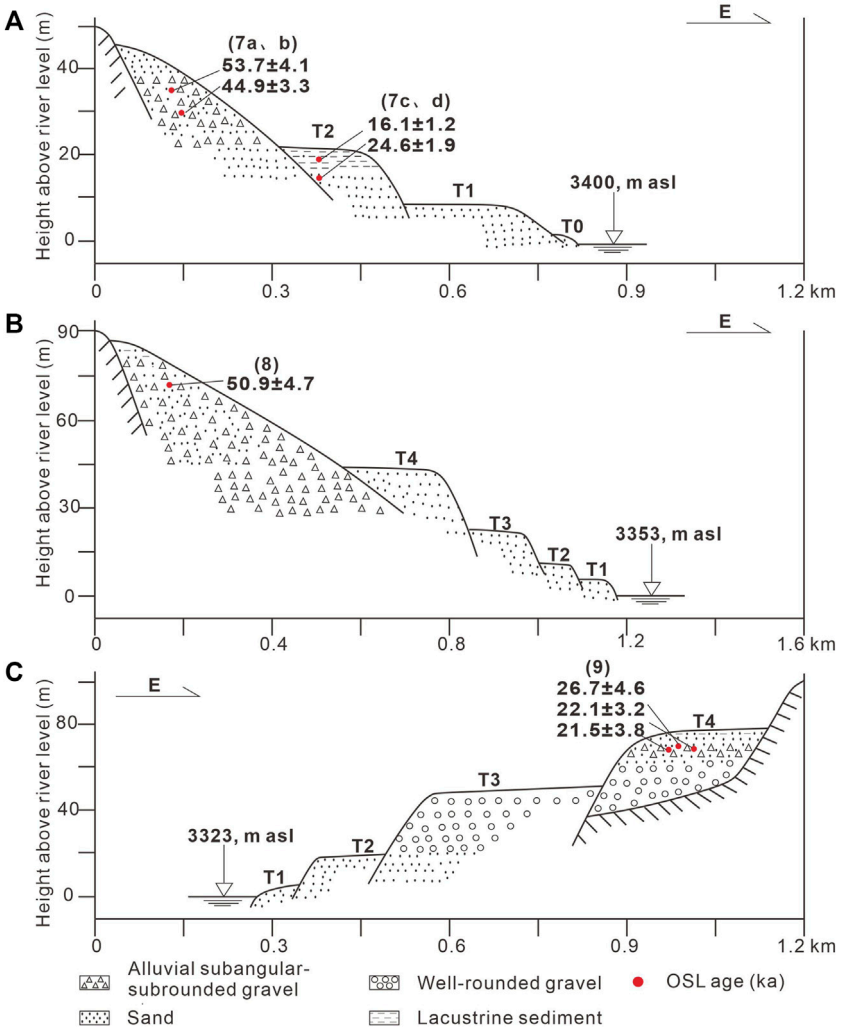

FIGURE 5
Schematic transverse sections of the terraces (sites 7–9), with dating data.

T3 terrace of sampling site 6 was 12.0 ± 0.9 ka (Figure 4B), which is roughly consistent with the age of the paleoflood sediments measured by Chen et al. (2017) in Maqu (Table 1). The Bayesian model established by the sample age of 10–20 m in the ZB13-C2 borehole (Zhao et al., 2020) yields its slope, i.e., the sedimentation rate ~0.2 mm/a, while the location of the ZK3 core is very close to that of ZB13-C2 core (Figure 1). The sedimentation rate in the Ruoergai Basin does not significantly vary between these two study sites, and the ^{14}C ages of the ZK3-^{14}C-2 and ZK3-^{14}C-4 samples measured herein are reliable. Thus, the ages of the ZK3-^{14}C-3 and ZK3-14 samples are considered as discrete values, and the age boundary between the lacustrine and swamp sediments can be estimated from the lacustrine sedimentary rate as ~55.3 ka.

4.2 Barrier dam

During the field investigation, we found three natural dams that are completely preserved, which were deposited on the accumulation terrace (Figure 5). The detailed descriptions are as follows.

Influenced by the stage uplift of the Tibetan Plateau since the Cenozoic, the Anyemaqen peaks were glaciated several times during the Quaternary period. The moraines and ice-water sediments formed around the Quaternary glaciations are preserved in the study area, which is geomorphologically reflected in the form of the ice trough valleys, moraine monopolies, and ice fen terraces (Figure 6A). An ice-mound terrace (Figure 6B) is present in the middle of Keshengxiang and Agetuo, where the sediments are mainly gravel and sand. The

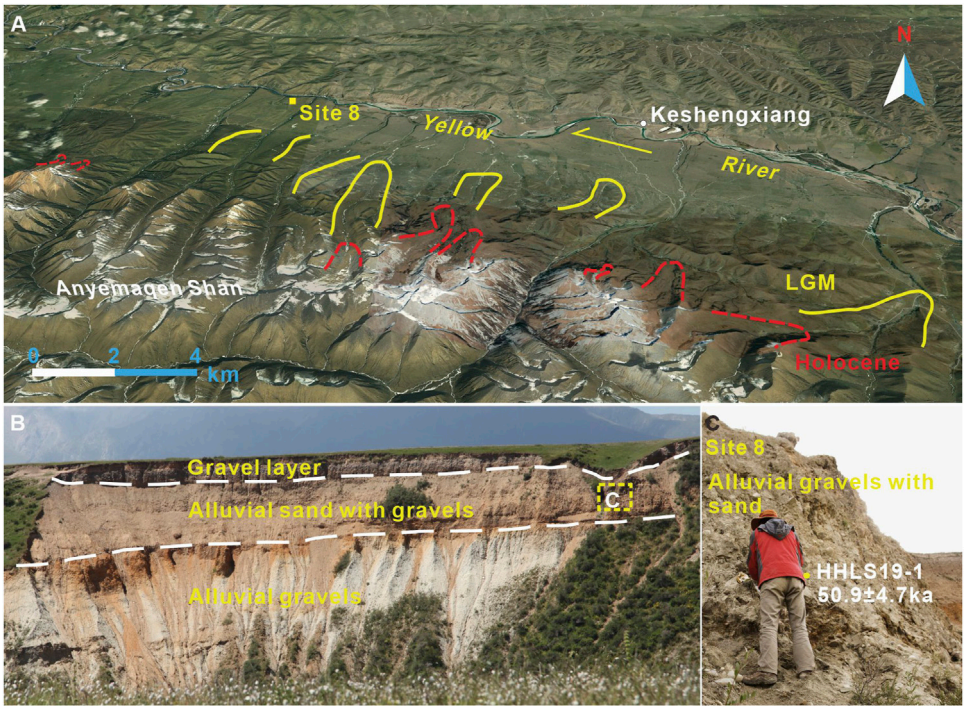

FIGURE 6
(A) Google Earth image showing the distribution of two periods of moraine ridges on the eastern side of the Anyemaqen Shan near Keshengxiang. **(B)** Photograph showing the sedimentary properties of sediments covering T5. **(C)** Photograph showing the sedimentary properties and OSL ages at site 8.

gravel has a certain roundness, comprises oblique bedding, and does not have a dual structure.

Site 8 is located on a flat and wide terrace, with a natural mixed accumulation and ~90 m of the profile is exposed. The entire site belongs to the back edge of the moraine monopoly accumulation of Anyemaqen Shan, which can be roughly divided into three layers (Figure 6B). The upper part is an ~2-m-thick gray-brown sand and gravel layer, and the middle part is an about 10-m-thick yellow-brown gravel layer, with a thin greenish gray sand lens body locally. The lower part is an ~78-m-thick grayish white gravel layer, and the gravel is mainly granite and sandstone. The OSL sample HHLS19-1 was collected at the depth of 3.5 m in the greenish-gray sand lens (Figure 6C).

Site 7 is located in the center between Maqu and Oula (Figure 1) at the intersection of the large diluvial fan from the Anyemaqen Shan and Xiqing Shan, outcropping the natural thick section of the alluvial–diluvial gravel accumulation. We conducted sample dating research on two typical sections with opposite gravel layers near the study site (Supplementary Figure S7A). The two profiles are located in the T3 terrace, with heights of ~42 m above river level. The first profile is about 25 m high (Supplementary Figure S7A, Section7a) and can be divided into three layers: the upper part is a 0.5-m-thick plough layer, and the middle part is a gravel layer containing yellowish brown fine sand lens. The occurrence of the gravel is 140°∠ 12°–13°. The gravel is not well rounded, with an average grain size of 2–3 cm and maximum grain size of 5 cm. The OSL sample MR19-1 (Supplementary Figure S7C) was collected at a depth of 13.3 m; The second profile is ~15 m high (Supplementary Figure S7F); its upper part is a 0.3-m-thick plough layer, and the middle part is a grayish brown fine gravel layer, with a gravel occurrence of 195°–200°∠12°. The gravel is not well rounded, and the average grain size is 2–3 cm, maximum grain size is 5 cm, and thickness is 11.5 m. The horizontal bedding in the yellow fine sand layer is clear, and the thickness is 0.1 m. The OSL sample MR19-2 (Supplementary Figure S7G) was taken at a depth of ~11.8 m. The gravel layer in the lower part is not well rounded, and its average particle size is 2–3 cm, maximum particle size is 5 cm, and thickness is ~3.5 m. In the artificial excavation profile (Sections 7c, 7d) near the highway, loess sedimentation and lacustrine sedimentation were observed. The profile can be divided into two layers, the upper part is a 1.5-m-thick loess layer (Supplementary Figure S7D), and the lower part is a yellow brown silt layer with clear horizontal bedding and a thickness of ~6 m (Supplementary Figure S7E). Two OSL samples (MR19-3 and MR19-4) were taken at depths of 2.7 and 7.1 m, respectively.

Site 9 is located in the transition position from the accumulation terrace to the bedrock terrace, which is a gentle slope formed by landslide accumulation near the canyon. It belongs to the T4 terrace, with a height of ~5 m (Supplementary Figure S8A). The upper part is a paleosol cultivation layer with a thickness of ~1.2 m, and the middle layer is ~0.7 m thick and has a horizontal gravel layer, which is mainly supported by debris. The sedimentary structure is relatively close, mainly composed of slate and sandstone, angular and sub-angular, with diameters ranging from 1 to 15 cm. The lower part comprises alluvium and diluvium and is 3.1 m thick. Additionally, the overall gravel grain size is relatively large, the sedimentary structure is relatively loose, and massive and oblique bedding has developed. The gravel is well rounded, with diameters ranging from 3 to 70 cm, and the gravel layer is locally interbedded with thin layers of grayish brown fine sand lens. Three OSL samples CYD19-2, 1, and 4 (Supplementary Figure S8B) were collected from the lens body at depths of 2.0, 2.4, and 2.7 m, respectively.

4.3 Canyon bedrock terrace

The downstream of the barrier dam is located in the bedrock canyon area. The river bed gradient is large, and the average slope is more than 60°. Only 1–2 grade bedrock terraces are present here. Site 10 has a hand-excavated profile with a thickness of ~5.7 m (Supplementary Figure S9A), which is overall a fluvial sedimentary profile. A 3.6-m-thick grayish-white loess layer is present in the upper part and a clayey chalk layer is present in the local area, and the NMT19-2 OSL sample was collected at a depth of 3.2 m. The middle part is a 0.7-m-thick yellowish-brown fine sand layer interbedded with a 0.2-m-thick gravel layer. The gravel is mainly supported by debris overall, mainly comprising slate and sandstone, with certain sorting and rounding. The gravel has a diameter of 3–10 cm and has weak bedding or oblique bedding, and the NMT19-1 OSL sample was collected at a depth of 3.9 m. The lower part is a 1.4-m-thick gravel layer, is mainly composed of slate and sandstone, has diameters ranging from 0.2 to 1 m, and has oblique bedding (Supplementary Figure S9B). The ages of the two fluvial sediments are 13.7 ± 1.7 and 12.9 ± 1.5 ka, respectively, indicating that the time of the Yellow River cutting in the downstream bedrock canyon area is ~14 ka.

5 Discussion

5.1 Geomorphic process of the outlet reach of the ruoergai Basin in the Late Quaternary

The geomorphological space-time evolution process of the Cairima-Ningmute reach of the Yellow River source since the Late Quaternary was reconstructed based on the new obtain dating results and previous ages (Li et al., 2011; Chen et al., 2017; Hu et al., 2018a; Liu et al., 2021), and three stages of evolution process were concluded as the follows (Figure 7):

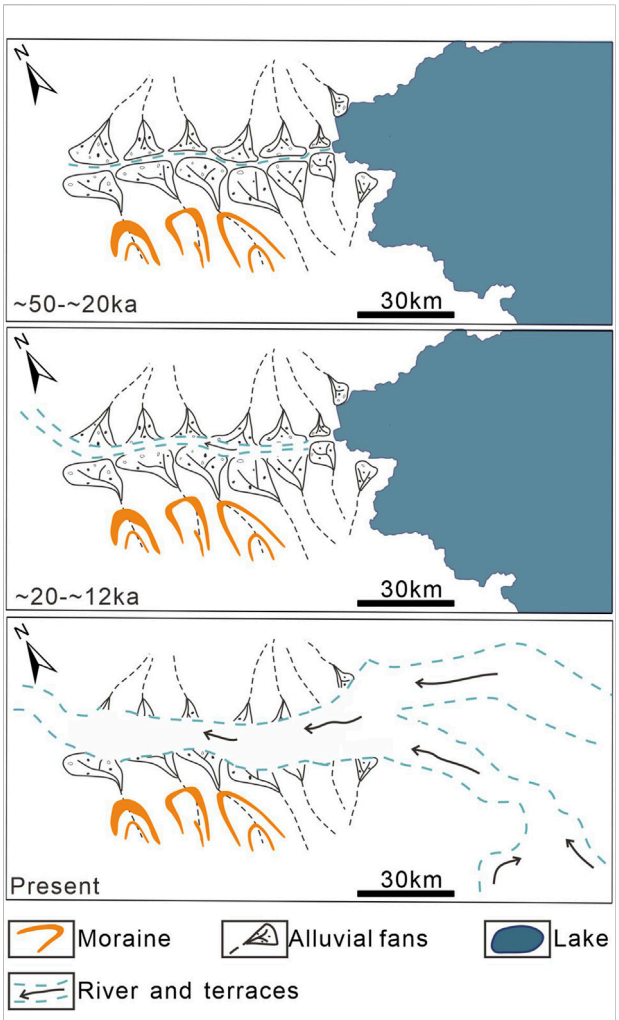

FIGURE 7
Map of the evolution of regional landscapes.

5.1.1 ~50–20 ka: Formation of the barrier dam

As shown in Figure 6C; Supplementary Figures S7C, S7G, S8B, the OSL dating results of 21.5–53.7 ka is roughly consistent with the ^{10}Be exposure age of ~20–51 ka of the oldest moraine in the Anyemaqen Shan glacial period in Owen et al. (2003). This indicates that large amounts of glacial sediments in Anyemaqen Shan and materials on the Xiqing Mountain were unloaded into the river valley through geological actions, such as glacial mudflows and alluvial flood sediments, resulting in the blockage of the river channel and the formation of a large barrier dam. Such serious events block the channel for a long time, and the data of the ZK03 core and other cores suggest that

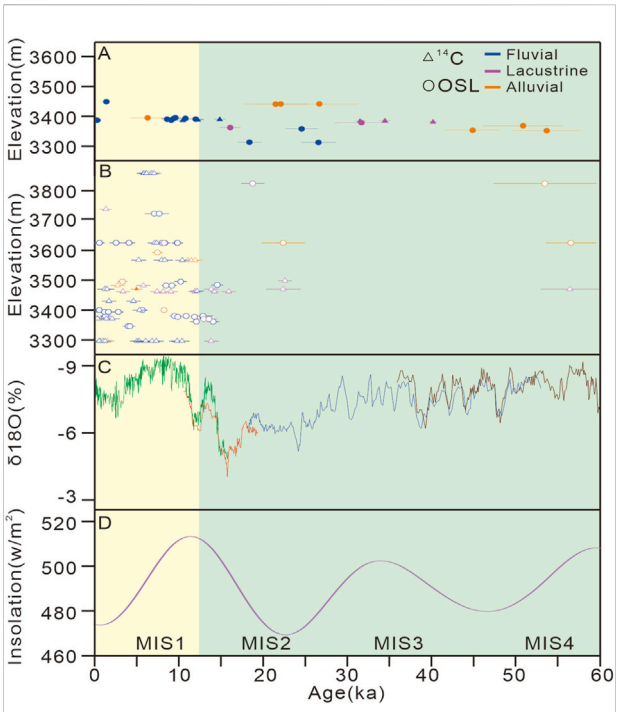

FIGURE 8
(A) Elevation–age plot of this study. **(B)** Elevation–age plot of previous studies in the study area. **(C)** Oxygen isotopic record of the Dongge–Hulu caves (Wang et al., 2005; Cheng et al., 2006). **(D)** Changes in insolation (June insolation at 30°N) (Sanchezgoni and Harrison, 2010), MIS = Marine Isotopic Stage, defined after Rind (1987) and Harrison and Sanchezgoni (2010).

the upstream of the Ruoergai Basin was a lake during this period (Chen et al., 1995; Zhao et al., 2020).

5.1.2 ~20–12 ka: Rapid migration of the Yellow River knickpoints

During this period, the downstream knickpoints rapidly migrated toward the source, and river terraces started developing on both sides of the main channel of the Yellow River. As shown in Supplementary Figure S9B, the chronological data show that the sedimentary age of the Yellow River on the highest terrace in the Maqu–Keshengxiang reach is 14.1–11.9 ka (Table 1). The formation ages of the terraces in the Maqu reach are mainly 1–2, 3–5, 7–10, and 12.5–15 ka (Li, 2010). As shown in Figures 5B; Supplementary Figure S6A, the transition from lacustrine to fluvial sediments at the outlet of the Ruoergai Basin is dated to ~12.0 ka (Sites 5 and 6), and the age of the lacustrine layer samples in the fluvial–lacustrine terrace within the Ruoergai Basin is 18.5 ± 1.5 ka. Based on the ages of these strata, it can be inferred that the knickpoints in the canyon area rapidly passed upstream at ~14 ka and passed to Maqu at ~12.0 ka, and the Ruoergai Basin was still in a paleolake state during this period.

5.1.3 Since ~12 ka: Cutting of the Yellow River into the Ruoergai Basin

As shown in Supplementary Figure S5, the ages of the fluvial sediments in the terraces of the Ruoergai Basin are 9.2–11.9 ka, and the age of the aeolian sediments near the Heihe River is 10.27 ± 0.81 ka (Hu et al., 2018a). The core data reveal that fluvial sediments in the Ruoergai Basin have been deposited since ~12 ka. These chronological data suggest that the highest fluvial terrace in the Ruoergai Basin probably formed at ~12 ka. During this period, the world entered the Holocene warm period; the humid climate, ice melting, and snow melting as well as the abundant rainfall enhanced the erosion and unloading ability of the rivers in the valley. The mixed accumulation body or alluvial fan body formed in the early period suffered from river erosion and destruction. The residual small weir body rapidly died out, the lake phase strata in the Ruoergai Basin suffered from erosion, the Ruoergai paleolake phase sediments were gradually replaced by river phase sediments, and the Yellow River connected to the Ruoergai Basin.

5.2 River evolution in relation to climate change

As shown in Figure 8A, the exposure age shows that the fluvial sediments of the Ruoergai Basin outlet reach at the source of the Yellow River were deposited after ~12.5 ka. The OSL ages suggest that the dam was deposited between ~50 and ~20 ka (Figures 8A,B), with lacustrine sedimentary aggradation occurring during the ~15–40 ka period in the Ruoergai Basin. Therefore, we propose that the most extensive dam in the outlet reach at the source of the Yellow River occurred during ~50–20 ka. The age of ~50 ka is consistent with MIS 3/MIS 4, when the Indian-Summer-Moon-dominated regions were controlled by humid and warm climatic conditions in the Dongge–Hulu caves (Wang et al., 2005; Cheng et al., 2006; Figures 8C,D), and the Indian monsoon precipitation may be 2–5 times more than the current one (Pachur et al., 1995; Jia et al., 2017). Glaciers are sensitive indicators of climate change, and the Anyemaqen Shan is precisely the most developed area of modern glaciers and Quaternary paleoglaciers in the northeastern Tibetan Plateau, where the glacier extent was much greater during MIS 3 than MIS 2 (Finkel et al., 2003; Shi et al., 2006). High lake surface records of many large lakes on the Tibetan Plateau and adjacent areas indicate that rainfall during 40–30 ka was 1.4–2 times greater than that at present (Shi et al., 2001). Based on the ice edge geomorphology observed in the Maqu valley and the buried ancient moraine dating results (Figures 6A–C), we assume that during ~50–20 ka, the glacial activities of Anyemaqen Shan as well as rainfall erosion and seepage weakened the stability of the moraine in Maqu valley. The weakening is conducive to the occurrence of alluvial flood accumulation, mudslides, and other geological processes under the action of external forces, resulting in

the formation of long periods of blocking and pseudo-terrace geomorphology in the Maqu River. The upstream Ruoergai Basin formed a barrier lake due to the blockage of the outlet. Various drilling data in the basin reveal the lacustrine sediments of this period. The region from the downstream of the barrier dam to Ningmute exhibit the typical characteristics of rocky mountain rivers with a large longitudinal profile gradient and a V-shaped river channel, which may be the geomorphological effect caused by the large-scale river blocking and barrier events in the alpine canyon area. During ~20–12.5 ka, which is consistent with the Last Ice Age, the expanding ice cap and valley glaciers on the Qinghai–Tibet Plateau began to retreat on a large scale (Li et al., 1991), rivers began strong anadromous erosion, and terraces began to extensively develop (as shown in Supplementary Figure S1). The fluvial sediments suggest that a paleolake burst through its dam after ~12.5 ka (Figures 8A,B), which is consistent with the Early Holocene period. During this time, the study area was controlled by relatively wet and warm climatic conditions in the Dongge–Hulu caves (Wang et al., 2005; Cheng et al., 2006) and ice melting, and abundant rainfall enhanced the erosion and unloading capacity of the valley rivers. Moreover, the mixed accumulation body or alluvial fan body formed in the early stage was completely destroyed by river erosion, the Ruoergai basin was replaced by fluvial sediments, and river terraces began to develop. The glacial-interglacial cycles during the Quaternary would generated repeated damming and cut-through of the Ruoergai Basin. The Ruoergai Basin should be connected with the lower reach before ~50 ka.

6 Conclusion

(1) According to the dating results of six ^{14}C and five OSL samples from shallow boreholes and surface terrace sections in the Ruoergai Basin, the basin was in a paleolake environment during ~50–12°ka, and the latest phase of fluvial–lacustrine transition took place at ~12°ka.

(2) Based on the analysis of sedimentology, geomorphology, and chronology in the study area, the dam-barrier model was first proposed to reconstruct the geomorphological evolution process of the Cairima–Ningmu reach. During the period of ~50–20°ka, the Maqu valley was blocked, forming a barrier dam, and the Ruoergai Basin formed a barrier lake. During ~20–12°ka, the knickpoints in the lower reaches rapidly migrated to the upper reaches, and terraces developed in the Maqu-Agetuo reach, while the Ruoergai basin was a shallow lake state without being cut. After ~12°ka, the paleo-dam was cut through, the sedimentation of the Ruoergai basin changed from lacustrine facies to fluvial facies, the Yellow River was connected, and fluvial terraces began to develop in the basin.

(3) Since the Late Quaternary, the Cairima–Ningmute section at the source of the Yellow River has undergone geomorphic evolution under the influence of tectonic activity and climatic change. The knickpoints zone of the Yellow River and the distinctive geomorphology of the Maqu reach are both under the control of the East Kunlun fault zone. The glacial debris flow from the Anyemaqen Shan filled the Maqu River valley during the last glacial epoch, and when the amount of silt buildup exceeded the rate of river erosion, a damming event occurred. During the last deglaciation period, with the melting of glaciers and the increase of the water volume, the barrier dam was eroded and cut down, and the Ruoergai Basin was eventually connected by the Yellow River.

Data availability statement

The original contributions presented in the study are included in the article/Supplementary Material, further inquiries can be directed to the corresponding author.

Author contributions

LS is responsible for field work, writing, drawing the Figures, and editing. PW is responsible for writing, editing and helpful comments. LS, PW, YG, RX, and BX are responsible for field work and drawing the Figures. GH and HW is responsible for constructive comments. JQ and HY are responsible for the laboratory dating. All authors contributed to the article and approved the submitted version.

Funding

This research was jointly financed by the National Natural Science Foundation of China (Grant No. 42072214), and the Special Topic one of 1:250,000 Active Fault Survey in Aba Prefecture: Determination of Quaternary Standard Stratigraphy and Establishment of Geomorphological Sequence in Aba Prefecture (including the Basin area).

Acknowledgments

We should like to thank H. L. Yang and A. M. Zhang for their help with the laboratory dating. We are grateful to the reviewers, their valuable comments and constructive suggestions significantly improved the quality of the manuscript.

Conflict of interest

Author RX was employed by the company Sichuan Institute of Geological Engineering Investigation Group Co. Ltd.

The remaining authors declare that the research was conducted in the absence of any commercial or financial relationships that could be construed as a potential conflict of interest.

Publisher's note

All claims expressed in this article are solely those of the authors and do not necessarily represent those of their affiliated organizations, or those of the publisher, the editors and the reviewers. Any product that may be evaluated in this article, or claim that may be made by its manufacturer, is not guaranteed or endorsed by the publisher.

Supplementary material

The Supplementary Material for this article can be found online at: https://www.frontiersin.org/articles/10.3389/feart.2022.1017597/full#supplementary-material

References

Aitken, M. J. (1998). *Introduction to optical dating: The dating of quaternary sediments by the use of photon-stimulated luminescence*. Clarendon Press.

Arnold, L. J., Roberts, R. G., Galbraith, R. F., and DeLong, S. B. (2009). A revised burial dose estimation procedure for optical dating of youngand modern-age sediments. *Quat. Geochronol.* 4 (4), 306–325. doi:10.1016/j.quageo.2009.02.017

Chen, F. H., Wang, S. M., Li, J. J., Shi, Y. F., Li, S. J., Cao, J. X., et al. (1995). Magnetostratigraphy of the zoige lake core in the qinghai-tibet plateau. *Sci. China (Series B)* 25 (7), 772–777.

Chen, J., Lu, W., Huang, G., Zhu, J., and Wang, J. (2017). Research on pulsed jet flow control without external energy in a blade cascade. *Energies* 10 (12), 2004. doi:10.3390/en10122004

Chen, Y. L., Huang, C. C., Zhang, Y. Z., Guo, Y. Q., Zhou, Y. L., and Zha, X. C. (2017). Study of the sedimentology and OSL dating of the Last Deglaciation paleoflood events along Maqu section in the source regions of the Yellow River. *J. Glaciol. Geocryol.* 39 (3), 549–562. doi:10.7522/j.issn.1000-0240.2017.0062

Cheng, H., Edwards, R. L., Wang, Y., Kong, X., Ming, Y., Kelly, M. J., et al. (2006). A penultimate glacial monsoon record from Hulu Cave and two-phase glacial terminations. *Geol.* 34 (3), 217–220. doi:10.1130/G22289.1

Craddock, W. H., Kirby, E., Harkins, N. W., Zhang, H., Shi, X., and Liu, J. (2010). Rapid fluvial incision along the Yellow River during headward basin integration. *Nat. Geosci.* 3 (3), 209–213. doi:10.1038/ngeo777

Duller, G. A. T. (2003). Distinguishing quartz and feldspar in single grain luminescence measurements. *Radiat. Meas.* 37, 161–165. doi:10.1016/S1350-4487(02)00170-1

Faershtein, G., Porat, N., Avni, Y., and Matmon, A. (2016). Aggradation–incision transition in arid environments at the end of the Pleistocene: An example from the Negev Highlands, southern Israel. *Geomorphology* 253, 289–304. doi:10.1016/j.geomorph.2015.10.017

Fan, P. L. (2021). *Late Quaternary alluvial sequences of the Chengdu Plain photochronological study*. Master's thesis in Chinese. Beijing, China: Capital Normal University.

Finkel, R. C., Owen, L. A., Barnard, P. L., and Caffee, M. W. (2003). Beryllium-10 dating of Mount Everest moraines indicates a strong monsoon influence and glacial synchroneity throughout the Himalaya. *Geology* 31 (6), 5612–6564. doi:10.1130/0091-7613(2003)031<0561:BDOMEM>2.0.CO;2

Galbraith, R. F. (2010). On plotting OSL equivalent doses. *Ancient TL* 28 (1), 1–10.

Harkins, N., Kirby, E., Heimsath, A., Robinson, R., and Reiser, U. (2007). Transient fluvial incision in the headwaters of the Yellow River, northeastern Tibet, China. *J. Geophys. Res.* 112 (F3), F03S04. doi:10.1029/2006JF000570

Harrison, S. P., and Sanchezgoni, M. F. (2010). *High-resolution pollen records and reconstruction of vegetation changes during Dansgaard-Oeschger events*. Special Issue of Quaternary Science Reviews.

Hu, G., Yi, C. L., Liu, J. H., Wang, P., Zhang, J. F., Li, S. H., et al. (2020). Glacial advances and stability of the moraine dam on mount namcha barwa since the last glacial maximum, eastern himalayan syntaxis. *Geomorphology* 365, 107246. doi:10.1016/j.geomorph.2020.107246

Hu, G., Yi, C., Zhang, J., Cao, G., Pan, B., Liu, J., et al. (2018). Chronology of a lacustrine core from lake linggo Co using a combination of OSL, 14C and 210Pb dating: Implications for the dating of lacustrine sediments from the Tibetan plateau. *Boreas* 47 (2), 656–670. doi:10.1111/bor.12291

Hu, G., Yu, L., Dong, Z., Lu, J., Li, J., Wang, Y., et al. (2018a). Holocene aeolian activity in the Zoige Basin, northeastern Tibetan plateau, China. *Catena* 160, 321–328. doi:10.1016/j.catena.2017.10.005

Huang, X., Lai, Z., Xu, L., Luo, L., Zhong, J., Xie, J., et al. (2022). Late Pleistocene lake overspill and drainage reversal in the source area of the Yellow River in the Tibetan Plateau. *Earth Planet. Sci. Lett.* 589, 117554. doi:10.1016/j.epsl.2022.117554

Institute of Geology; China Earthquake Administration, and Sichuan Geological Engineering Exploration Institute Group Co (Forthcoming 2022). *Report on the quaternary standard stratigraphy and geomorphic sequence establishment project in Aba prefecture (including the Basin region). Aba prefecture (including the Basin) 1: 250,000 Active Fault Survey project*.

Jia, L., Hu, D., Wu, H., Zhao, X., Chang, P., You, B., et al. (2017). Yellow River terrace sequences of the gonghe–guide section in the northeastern qinghai–tibet: Implications for plateau uplift. *Geomorphology* 295, 323–336. doi:10.1016/j.geomorph.2017.06.007

Kirby, E., Harkins, N., Wang, E., Shi, X., Fan, C., and Burbank, D. (2007). Slip rate gradients along the eastern Kunlun fault. *Tectonics* 26 (2), 1–16. doi:10.1029/2006TC002033

Korup, O., and Montgomery, D. R. (2008). Tibetan Plateau river incision inhibited by glacial stabilization of the Tsangpo Gorge. *Nature* 455 (7214), 786–789. doi:10.1038/nature07322

Lai, Z. P., Zöller, L., Fuchs, M., and Brückner, H. (2008). Alpha efficiency determination for OSL of quartz extracted from Chinese loess. *Radiat. Meas.* 43 (2-6), 767–770. doi:10.1016/j.radmeas.2008.01.022

Lang, K. A., Huntington, K. W., and Montgomery, D. R. (2013). Erosion of the Tsangpo gorge by megafloods, eastern himalaya. *Geology* 41 (9), 1003–1006. doi:10.1130/G34693.1

Li, C. X. (2010). Late Quaternary long-term slip behavior in the eastern segment of the East Kunlun fault zone (Maqin-Maqu). *Recent Dev. World Seismol.* 375 (03), 36–39. doi:10.3969/j.issn.0235-4975.2010.03.010

Li, C. X., Xu, X. W., Wen, X. Z., Zheng, R. Z., Chen, G. H., Yang, H., et al. (2011). Rupture segmentation and slip partitioning of the mid-eastern part of the Kunlun Fault, north Tibetan Plateau. *Sci. China Earth Sci.* 41 (9), 1730–1745. doi:10.1007/s11430-011-4239-5

Li, J. J., Zhang, J. L., and Guo, Y. T. (2016). Chronostratigratigraphic classification of zoige basin since late Pleistocene and its tectonic-climate significance. *Seismol. Geol.* 38 (4), 950–963. doi:10.3969/j.issn.0253-4967.2016.04.012

Li, L. J., Zhou, S. Z., and Pan, B. T. (1991). The problems of Quaternary glaciation in the eastern part of Qinghai-Xizang Plateau. *Quat. Sci.* 11 (3), 193–203.

Liu, J. F., Chen, J., Yin, J. H., Lu, Y. C., Murray, A. S., Chen, L. C., et al. (2010). OSL and AMS dating of the penultimate earthquake at the leigu trench along the beichuan fault, longmen Shan, in the northeast margin of the Tibetan plateau. *Bull. Seismol. Soc. Am.* 100, 2681–2688. doi:10.1785/0120090297

Liu, W., Carling, P. A., Hu, K., Wang, H., Zhou, Z., Zhou, L., et al. (2019). Outburst floods in China: A review. *Earth-Science Rev.* 197, 102895. doi:10.1016/j.earscirev.2019.102895

Liu, Y., Wang, X., Su, Q., Yi, S., Miao, X., Li, Y., et al. (2021). Late Quaternary terrace formation from knickpoint propagation in the headwaters of the Yellow River, NE Tibetan Plateau. *Earth Surf. Process. Landf.* 46 (14), 2788–2806. doi:10.1002/esp.5208

Lu, Y. C., Wang, X. L., and Wintle, A. G. (2007). A new OSL chronology for dust accumulation in the last 130, 000 yr for the Chinese Loess Plateau. *Quat. Res.* 67 (1), 152–160. doi:10.1016/j.yqres.2006.08.003

Ouimet, W. B., Whipple, K. X., Royden, L. H., Sun, Z., and Chen, Z. (2007). The influence of large landslides on river incision in a transient landscape: Eastern margin of the Tibetan Plateau (Sichuan, China). *Geol. Soc. Am. Bull.* 119 (11-12), 1462–1476. doi:10.1130/B26136.1

Owen, L. A., Finkel, R. C., Haizhou, M., Spencer, J. Q., Derbyshire, E., Barnard, P. L., et al. (2003). Timing and style of late quaternary glaciation in northeastern tibet. *Geol. Soc. Am. Bull.* 115 (11), 1356–1364. doi:10.1130/B25314.1

Pachur, H. J., Wünnemann, B., and Zhang, H. (1995). Lake evolution in the tengger desert, northwestern China, during the last 40, 000 years. *Quat. Res.* 44 (2), 171–180. doi:10.1006/qres.1995.1061

Pan, B., Su, H., Hu, Z., Hu, X., Gao, H., Li, J., et al. (2009). Evaluating the role of climate and tectonics during non-steady incision of the Yellow River: Evidence from a 1.24 Ma terrace record near lanzhou, China. *Quat. Sci. Rev.* 28 (27-28), 3281–3290. doi:10.1016/j.quascirev.2009.09.003

Pan, B. T., Li, J. J., and Zhou, S. Z. (1993). *A preliminary study on that development history of the uppermost reach of the yellow river. See: Geomorphological process and environment*. Beijing: Seismological Press, 17–21.

Prescott, J. R., and Hutton, J. T. (1994). Cosmic ray contributions to dose rates for luminescence and ESR dating: Large depths and long-term time variations. *Radiat. Meas.* 23, 497–500. doi:10.1016/1350-4487(94)90086-8

Rees-Jones, J. (1995). Optical dating of young sediments using fine-grain quartz. *Ancient TL* 13 (2), 9–14.

Rind, D. (1987). The doubled CO2 climate: Impact of the sea surface temperature gradient. *J. Atmos. Sci.* 44 (6), 3235–3268. doi:10.1175/1520-0469(1987)044<3235:tdccio>2.0.co;2

Sanchezgoni, M. F., and Harrison, S. P. (2010). Millennial-scale climate variability and vegetation changes during the Last Glacial: Concepts and terminology. *Quat. Sci. Rev.* 29 (21-22), 2823–2827. doi:10.1016/j.quascirev.2009.11.014

Sheng, H. Y., Zhai, Q. M., and Guo, Z. Y. (2007). Study on quaternary stratigraphy of the Yellow River basin in sichuan province. *Yellow River* 268 (12), 3–5. CNKI:SUN:RMHH.0.2007-04-001.

Shi, Y., Liu, S., Shangguan, D., Li, D., and Ye, B. (2006). Peculiar phenomena regarding climatic and glacial variations on the Tibetan Plateau. *Ann. Glaciol.* 43, 106–110. doi:10.3189/172756406781812267

Shi, Y., Yu, G., Liu, X., Li, B., and Yao, T. (2001). Reconstruction of the 30–40 ka BP enhanced Indian monsoon climate based on geological records from the Tibetan Plateau. *Palaeogeogr. Palaeoclimatol. Palaeoecol.* 169 (1-2), 69–83. doi:10.1016/S0031-0182(01)00216-4

Sichuan Geological Survey Institute (2008). *1: 250,000 regional geological survey report of Ruoergai county area*.

Stroeven, A. P., Hättestrand, C., Heyman, J., Harbor, J., Li, Y. K., Zhou, L. P., et al. (2009). Landscape analysis of the Huang He headwaters, NE Tibetan plateau—patterns of glacial and fluvial erosion. *Geomorphology* 103 (2), 212–226. doi:10.1016/j.geomorph.2008.04.024

Stuiver, M., Reimer, P. J., and Reimer, R. W. (2020). *CALIB 8.2 [WWW program]*.

Thrasher, I. M., Mauz, B., Chiverrell, R. C., and Lang, A. (2009a). Luminescence dating of glaciofluvial deposits: A review. *Earth-Science Rev.* 97 (1-4), 133–146. doi:10.1016/j.earscirev.2009.09.001

Thrasher, I. M., Mauz, B., Chiverrell, R. C., Lang, A., and Thomas, G. S. P. (2009b). Testing an approach to OSL dating of Late Devensian glaciofluvial sediments of the British Isles. *J. Quat. Sci.* 24 (7), 785–801. doi:10.1002/jqs.1253

Wang, Y., Cheng, H., Edwards, R. L., He, Y., Kong, X., An, Z., et al. (2005). The Holocene asian monsoon: Links to solar changes and north atlantic climate. *Science* 308 (5723), 854–857. doi:10.1126/science.1106296

Wang, Y. F., Wang, S. M., Xue, B., Ji, L., Wu, J. L., Xia, W. L., et al. (1995). Sedimentological evidence for the age of the ancient Ruoergai lake captured by the Yellow River. *Chin. Sci. Bull.* 40 (8), 723–725.

Wu, J. L., Wang, S. M., Pan, H. X., and Xia, W. L. (1997). Paleoclimate characteristics recorded by lacustrine carbonate isotopes since 140 ka in RM core, Eastern Tibetan Plateau. *Sci. China (Series D)* 27 (3), 255–259. doi:10.1007/s00376-997-0061-6

Wu, Q., Zhao, Z., Liu, L., Granger, D. E., Wang, H., Cohen, D. J., et al. (2016). Outburst flood at 1920 BCE supports historicity of China's Great Flood and the Xia dynasty. *Science* 353 (6299), 579–582. doi:10.1126/science.aaf0842

Xue, B., Wang, S. M., Wu, J. L., and Qian, J. L. (1999). Palaeoclimate of northeastern qinghai-xizang (tibet) Plateau since last interglaciation –A case study from core RM of the zoige basin. *Oceanol. Limnologia Sinica* 30 (3), 327–332. CNKI:SUN:HYFZ.0.1999-03-016.

Yang, H., Chen, J., Porat, N., Li, T., Li, W., and Xiao, W. (2017). Coarse versus fine-grain quartz optical dating of the sediments related to the 1985 Ms7. 1 Wuqia earthquake, northeastern margin of the Pamir salient, China. *Geochronometria* 44 (1), 299–306. doi:10.1515/geochr-2015-0075

Zhang, H., Kirby, E., Pitlick, J., Anderson, R. S., and Zhang, P. (2017). Characterizing the transient geomorphic response to base-level fall in the northeastern Tibetan Plateau. *J. Geophys. Res. Earth Surf.* 122 (2), 546–572. doi:10.1002/2015JF003715

Zhang, J. F., Zhou, L. P., and Yue, S. Y. (2003). Dating fluvial sediments by optically stimulated luminescence: Selection of equivalent doses for age calculation. *Quat. Sci. Rev.* 22 (10-13), 1123–1129. doi:10.1016/S0277-3791(03)00054-4

Zhang, X. B., Liu, H., Wang, S. J., Liu, W. M., and Xue, W. X. (2018). The formation, evolution and transfixion time of the Yellow River and the Yangtze River. *Mt. Res.* 36 (5), 661–668. doi:10.16089/j.cnki.1008-2786.000362

Zhang, Y. Q., Li, H. L., and Li, J. (2016). Impact of the 30–40 ka B.P. Warm-Humid climate in tibet on the geo-environment of the deep-incised river valleys in west sichuan. *Acta Geosci. Sin.* 37 (4), 481–492. doi:10.3975/cagsb.2016.04.10

Zhao, Q., Thomsen, K. J., Murray, A. S., Wei, M., Pan, B., Song, B., et al. (2015). Testing the use of OSL from quartz grains for dating debris flows in Miyun, northeast Beijing, China. *Quat. Geochronol.* 30, 320–327. doi:10.1016/j.quageo.2015.03.007

Zhao, Q. Y., Xiao, G. Q., and Li, H. (2019). Valley features of the Yellow River source area and its implications for the formation and evolution of the upstream. *Quat. Sci.* 39 (2), 339–349. doi:10.11928/j.issn.1001-7410.2019.02.07

Zhao, Y., Tzedakis, P. C., Li, Q., Qin, F., Cui, Q., Liang, C., et al. (2020). Evolution of vegetation and climate variability on the Tibetan Plateau over the past 1.74 million years. *Sci. Adv.* 6 (19), eaay6193. doi:10.1126/sciadv.aay6193

Zheng, B. X., and Wang, S. M. (1996). A study on the paleo-glaciation and paleo-environment in the source area of the Yellow River. *J. Glaciol. Geocryol.* 18 (3), 20–28.

Zhou, M. Z. (1959). Quaternary mammalian fossils from Aba Tibetan autonomous prefectur. *Quat. Sci.* 2 (1), 6–13.

Zong, G. F., Xu, Q. Q., and Chen, W. Y. (1985). Note on the late Pleistocene mammalian fossils in the apa zangzu zizhizhou. *Vertebr. Palasiat.* 23 (2), 161–166. CNKI:SUN:GJZD.0.1985-02-004.